RASĀYAN *J. Chem.*
Vol. 19 | No. 3 | 1902-1918 | July-September | 2026
ISSN: 0974-1496 | e-ISSN: 0976-0083 | CODEN: RJCABP
http://www.rasayanjournal.com
http://www.rasayanjournal.co.in

INVESTIGATION OF HYDROGEN-GRAPHENE OXIDE SYNERGY ON COMBUSTION AND EMISSION CHARACTERISTICS OF WASTE PLASTIC OIL-DIESEL BLENDS

R.V. Kadupu[1,✉], K. S. Jafar[2] and P. V. Elumalai[3]

[1]Research Scholar, Department of Mechanical Engineering, Faculty of Engineering and Technology, Annamalai University, Chidambaram-608002, Tamil Nadu, India
[2]Department of Mechanical Engineering, Government College of Engineering, Dharmapuri-636704, Tamil Nadu, India
[3]Department of Mechanical Engineering, Aditya University, Surampalem-533437, Andhra Pradesh, India
✉Corresponding author: varma370@gmail.com

ABSTRACT

Waste plastic oil (WPO) from pyrolysis provides a waste-to-energy pathway for compression-ignition engines, yet its lower cetane quality, broad boiling range, and aromatic content delay ignition and intensify soot formation. The objective of the current study is to evaluate the coupled effects of hydrogen and graphene oxide (GO) on combustion phasing, thermal efficiency, and regulated emissions of a WPO-diesel blend. Graphene oxide was dispersed at 100 ppm via solvent-assisted probe ultrasonication and nano fuel stability was verified through UV-Vis monitoring, for which absorbance drift showed less than 5% over seven days. Engine tests were carried out on a four-stroke, single-cylinder, direct-injection diesel engine at 25-100% load with a 10% hydrogen energy share. At full load, WPO20+H_2+GO achieved a brake thermal efficiency of 34.4%, nearly 3.6% above WPO20 and 2.3% higher than diesel. Brake specific fuel consumption had fallen from 281 g kW/h for WPO20 to 238 g kW/h, while smoke decreased from FSN 6 to FSN 1. Carbon monoxide and unburned hydrocarbon emissions had been reduced to 0.08% and 2.5 ppm, respectively. NOx reached 1500 ppm with hydrogen alone but decreased to 1450 ppm when graphene oxide was added. These findings demonstrated that hydrogen and graphene oxide co-enrichment offered a practical combustion upgrade strategy for recovering the performance of plastic-derived fuels. Future work should target EGR-assisted NOx mitigation, injector deposit tracking, and multicylinder validation. The current study aligns with SDG 7 (Affordable Clean Energy) by contributing to improved energy efficiency and alternative fuel development.

Keywords: Waste Plastic Oil, Graphene Oxide Nanoparticles, Hydrogen, Fuel Characterization, FTIR, UV-Visible Spectroscopy.

RASĀYAN *J. Chem.*, Vol. 19, No.3, 2026

INTRODUCTION

The rapid depletion of fossil fuel sources, along with recent geopolitical conflicts and growing environmental impacts, has become a serious global concern. In response, there has been a growing focus on the exploration of alternative fuels for IC engines. Fuels derived from plastic waste and other organic matter have become popular as partial diesel alternatives, offering dual advantages of reducing reliance on traditional fossil fuels and mitigating challenges associated with plastic waste management and its associated environmental impacts. Pyrolytic oil produced from plastic waste is a hydrocarbon-rich fuel with a calorific value and physicochemical properties near to those of conventional diesel fuel. This makes it an attractive alternative for a direct pathway to convert into motor fuel. Despite its benefits, its direct usage is limited by several practical challenges. Waste plastic oil typically exhibits a wide boiling range, higher aromatic content and a lower cetane number compared to diesel. These properties hinder combustion performance by delaying heat release from the optimum crank angle and increasing soot formation.[1] Even though certain improvements are achievable; they remain susceptible to fuel volatility and spray characteristics. Strategies such as incorporating oxygenated additives and CRDI-based injection

http://doi.org/10.31788/RJC.2026.19310019

methods can enhance the plastic oil substitution.[2] Distilled WPO can attain energy density similar to diesel, but precise blending control is required due to variation in density and flash point depression.[3] Thermodynamic analysis of plastic pyrolysis oil diesel blends indicated that power output is largely maintained at lower blending ratios, but exergy and sustainable performance tend to decline as the proportion of plastic oil is increased.[4] Across the broader evidence, plastic-derived fuel blends require suitable supplementary fuels or additives to improve combustion and mitigate soot emissions. Nanoparticle-based fuel additives have emerged as an effective strategy to mitigate the slow oxidation kinetics of low cetane alternative fuels. The incorporation of nano-oxygenated additives into plastic pyrolysis oil has demonstrated improved combustion characteristics, although maintaining uniform and stable dispersion of nanoparticles into the fuel matrix has been flagged as an unresolved issue.[5] Graphene oxide nanoparticles, owing to their inherent oxygen-functionalized carbon framework, high surface area and catalytic activity, have been found to shorten the combustion duration and suppress carbon monoxide and soot formation. However, an important finding was that increasing the nanoparticle dosage beyond an optimum level did not yield further performance.[6] Establishing a stable graphene oxide (GO) suspension in dairy scum biodiesel needs surfactant-assisted ultrasonication along with UV-Visible spectroscopy for validation, emphasizing that dispersion quality is an essential prerequisite.[7] Ternary diesel-WPO-vegetable oil formulations had similarly been explored to combine waste recovery with renewable oxygenated components.[8] In the case of palm biodiesel, the combined action of GO nanoplatelets and dimethyl carbonate revealed that the effect of nano fuel stability influences not only emission characteristics but also tribological properties, thereby introducing injector wear choking.[9]

Table-1: Recent Studies on Waste-Derived Blended Fuels, Hydrogen and Nano Additives in Diesel Combustion

Reference	Objective	Methodology	Materials	Key Findings	Relevance to Current Study
Sekar, 2025	Upgrade pyrolysis oil combustion	Engine tests with H_2, Ce_2O_3	Pyrolysis oil, H_2, Ce_2O_3	Combustion, CO, HC	Closest H_2-nano pyrolysis analogue.[12]
Anand & Debbarma, 2024	Assess injection timing with H_2 - WPO	CRDI tests, varied timing	WPO blends, H_2, timing	Phasing control; Smoke	Supports H_2 - WPO calibration logic.[13]
Özer *et al*., 2025	Evaluate WTPO-HHO dual fuel	Energy, Exergy, Environ-Economic	WTPO blends, HHO rates	Efficiencies, Env. cost	Gaseous enrichment compromises.[14]
Wu *et al.,* 2024	Replace diesel using WTPO-H_2	Constant H_2 intake experiments	Waste tyre oil, diesel, H_2	Performance, Particulates	Pyrolysis oil H_2 coupling.[15]
Das et al., 2025	Optimize WPO additives, emissions	Pollution-cost analysis	WPO, ethanol, nanographene	CO, HC, NOx Costs	Links additives with WPO.[16]
Kumar *et al.,* 2024	Optimize PPO nano-fuel parameters	RSM with validation trials	PPO, Al_2O_3, CR, timing	Desirability, Errors	Parametric optimization guide.[17]
Ma *et al*., 2024	Compare carbon nano additives	DI engine load experiments	GO, MG, methanol-diesel	BTE, CO, HC, Smoke	Carbon-nano combustion data.[18]
Hammad *et al.*, 2024	Improve biodiesel with GO	Four-stroke diesel engine tests	Jatropha biodiesel, ethanol, GO	Torque, HC, NOx	Reduced-GO emission potential.[19]
Megiso *et al.*, 2025	Assess GO microalgal biodiesel	Characterization + engine test	Ulva biodiesel, GO, B5–B25	Stability, Pollutants	GO nanofuel preparation support.[20]

Comparative analysis of GO and graphene nanoplatelet tests demonstrated superior smoke reduction, although injector wear and filtration checks were not comprehensively examined.[10] Furthermore, hydrogen enrichment offers a new alternative pathway characterized by premixed flame propagation,

which enhances combustion stability and reduces carbon emissions but at the expense of elevated NOx emissions and high pressure rise unless effectively controlled with appropriate additives.[11]

Most studies are conducted under steady-state load sweep conditions on constant-speed compression ignition engines, where key parameters such as brake thermal efficiency (BTE), brake specific fuel consumption (BSFC), in-cylinder pressure, heat release rate, NOx, carbon monoxide (CO), hydrocarbon (HC), and smoke are measured directly. Analytical and statistical methods such as response surface methodology (RSM), exergy analysis, sustainability indicators and pollution cost models are typically used as supporting frameworks. A consistent trend reported in the literature indicates that nanoparticles supply oxygen during combustion, implying clean combustion and low soot formation. Variations among studies largely arise from differences in fuel type, hydrogen delivery, injection timing strategy and nanofuel chemistry; dosage and stability are systematically evaluated. The research emphasis is moving from single additive fuel substitution toward integrated combustion enhancement strategies. The tyre and plastic pyrolysis oils are no longer used solely as diesel extenders; instead, they have been combined with oxygenated nanoparticles, gaseous fuels and optimized injection strategies to the engine efficiency and reduce emissions. Among various nano additives, graphene-based nano additives have gained particular attention due to their large surface area, oxygen functional groups and non-metallic nature. Nevertheless, the practical application depends on proven dispersion stability and regulated dosing. In parallel, hydrogen enrichment paves the new ways to accelerate the burn rate of fuels that typically suffer from low cetane and calorific value. When hydrogen is inducted into WPO-fuelled CRDI engines, BTE was improved, although NOx emissions remained a persistent penalty.[21] A similar BTE-NOx trade-off had been observed with waste biodiesel enriched with hydrogen.[22] Existing studies do not adequately address the coupled behavior of WPO-diesel blends when hydrogen induction and graphene oxide dosing are applied together within a single controlled framework. Research on plastic oil largely evaluates blend viability but partially addresses persistent challenges such as ignition delay and smoke-prone diffusion combustion. Similarly, most of the nanoparticle-based findings on biodiesel-diesel blends cannot be directly applied to waste plastic oil blends because the fuel chemistry, aromatic loading and dispersion environment are different. Hydrogen dual-fuel investigations demonstrated enhanced combustion and reduced carbon emissions, but NOx and pressure rise intensity escalate unless a softening agent is incorporated into the fuel matrix. The parameter ranges, additive preparation protocols, stability verification methods and optimization depth vary widely across published work, making it unclear whether hydrogen and GO act cooperatively, antagonistically or simply additively when combined in WPO combustion. In contrast, the present work treats hydrogen induction and GO dosing as a coupled WPO upgrading strategy rather than two independent enhancement methods. It evaluates WPO-diesel blends under constant engine calibration, with controlled hydrogen energy shares of 0-10% and low ppm GO concentrations of 100 ppm. It systematically links fuel preparation, nano fuel stability assessment, combustion phasing, pressure rise behavior, thermal efficiency and regulated emissions within a single experimental framework. The design directly targets the unresolved balance between smoke suppression, CO/HC oxidation, thermal efficiency recovery, NOx control, and it establishes a basis for later calibration work by separating the role of hydrogen (heat-release phasing) from that of GO (ignition-delay shortening, soot oxidation, combustion intensity softening). The objective of the current study is to evaluate the joint effect of hydrogen induction and graphene oxide nanoparticle dosing on stability, performance, combustion behavior and emission characteristics of waste plastic oil-diesel blends in a CI engine. The present study aligns with the objectives of SDG-7 (Affordable and Clean Energy) and SDG-13 (Climate Action) through waste-to-energy generation and development of low-carbon emission strategies and reducing plastic waste-associated environmental impacts.

EXPERIMENTAL

Materials

Commercial petroleum diesel served as the reference liquid fuel and was designated D100. Waste plastic oil was derived from mixed polyolefin plastic waste through thermal pyrolysis followed by fractional distillation to isolate the diesel-range liquid fraction. The distilled waste plastic oil was blended with diesel on a volumetric basis to prepare blend WPO20 (80 % diesel and 20% waste plastic oil), and

graphene oxide nanoparticles were used as the fuel-borne nanomaterial, and Span 80 was used as a non-ionic surfactant at 0.1% v/v. Analytical grade ethanol was used solely as a wetting and dispersion medium and was removed before engine testing. The principal fuel properties are given in Table-2. All liquid fuels were stored in sealed borosilicate glass bottles at 298 ± 2 K before use, and all preparation steps were carried out at 296 ± 2 K and 50 ± 10% relative humidity.

Table-2: Properties of Diesel and WPO-Diesel Blends Used for Testing

Fuel blend	Density (kg/m^3)	Kin. Viscosity (m^2/s)	LHV (MJ/kg)	Cetane	Flash point (K)
Diesel (D100)	830	2.6×10^{-6}	43.0	50	335
WPO20	836	3.1×10^{-6}	42.4	46	327
Hydrogen	0.082	1.10×10^{-4}	120	-	-

Nano fuel Preparation

Graphene oxide was dispersed in the selected WPO diesel blend at a fixed concentration of 100 mg/L (100 ppm). The required mass of graphene oxide was first wetted with ethanol and subjected to probe ultrasonication for 1200 s in pulsed mode. The pre-dispersed fuel was transferred into the base fuel under magnetic stirring, followed by a second ultrasonication stage of 1800 s to ensure uniform dispersion. The prepared mixture was maintained at 323 K in a thermostatic bath until ethanol removal was completed, after which it was cooled to ambient temperature and sealed. The nanoparticle dispersion sequence is presented in Fig.-1.

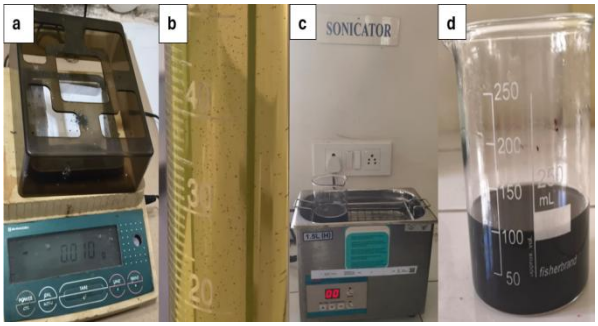

Fig.-1: Graphene Oxide Nanoparticle Dispersion Sequence for WPO-Diesel Nano Fuel Preparation
(a.) GO 100ppm, (b.) GO Dosing with D80WPO20, (c.) Sonication d. D80WPO20GO100ppm

Structural Analysis of Fuel Samples

Three fuel samples were prepared, such as pure diesel, WPO20D80, and WPO20D80+GO 100 ppm, to carry out structural analysis using FTIR and UV-Vis spectrophotometry. Pure diesel was used as a blank (reference) in the UV-Vis spectrometer, and WPO20D80+GO 100ppm used as the sample.

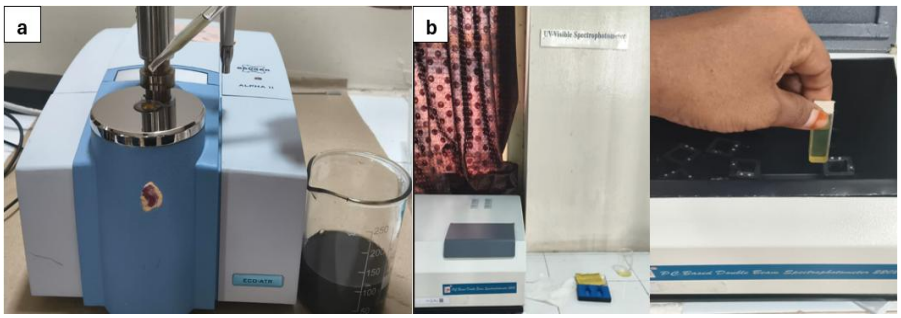

Fig.-2: Analytical Instruments used for Fuel Characterization (a) FTIR (b) UV-Visible Spectrophotometer

Figure-2(a) shows that Fourier Transform Infrared Spectroscopy (FTIR) was employed to detect functional groups, confirm blending, and study chemical interactions between plastic oil, diesel, and nano additives by analyzing infrared absorption spectra. The spectra were recorded across the range of 4000-400 cm^{-1}. Figure-2(b) shows, UV-Visible spectrophotometer is a simple and reliable technique for analyzing alternative fuel formulations. It effectively characterizes fuel samples and confirms the

presence of aromatic compounds and improved interactions within the fuel matrix. The absorbance spectral data were collected over a wide range of wavelengths from 200-800 nm using a double-beam spectrophotometer.

Stability Monitoring

Nanofuel stability was monitored without agitation for seven days using visual inspection and UV-Vis spectrophotometry. Absorbance was recorded at a fixed wavelength corresponding to the maximum absorbance of the nanoparticle suspension. The stability index (SI) was calculated from the normalized absorbance drift, as shown in Equation (1).

$$SI = \left(1 - \frac{|A_0 - A_t|}{A_0}\right) \times 100 \quad (1)$$

In Equation (1), SI is the stability index expressed as a percentage (%), A_0 is initial absorbance, A_t is absorbance time t. Absorbance is dimensionless.

Hydrogen Supply, Safety and Metering

Hydrogen was supplied from a cylinder via a two-stage pressure regulator, non-return valve, wet flame arrestor and calibrated mass flow controller. The supply, safety, and metering arrangement is presented in Fig.-3. Hydrogen was supplied into the intake air via a stream upstream of the inlet port. Hydrogen energy share set points of 0, 5, and 10% were imposed by regulating the hydrogen mass flow rate according to Equation (2).

$$x_{H_2} = \frac{\dot{m}_{H_2} \cdot LHV_{H_2}}{\dot{m}_{H_2} \cdot LHV_{H_2} + \dot{m}_l \cdot LHV_l} \quad (2)$$

Fig.-3: Hydrogen Supply, Safety and Flow Metering Arrangement

In Equation (2), x_{H_2} represents the hydrogen energy share (dimensionless). $\dot{m}_{H_2}$ and $\dot{m}_l$ indicates the mass flow rate of hydrogen and liquid fuel, respectively, expressed in kg/s. LHV_{H_2} and LHV_l are the lower heating values of hydrogen and liquid fuel, respectively and are expressed in J/kg.

Engine Setup and Operating Conditions

Engine experiments were undertaken on a 4-stroke single-cylinder water-cooled compression ignition engine coupled with an eddy current dynamometer. The schematic and photographic layout of the experimental facility is presented in Fig.-4.

The engine operating conditions and boundary settings were listed in Table-3. The engine was operated at 25%, 50%, 75% and 100% load at a fixed speed of 25 s^{-1}. The dynamometer held speed within ±0.5 s^{-1}, so load comparisons are reasonably clean. The coolant temperature was maintained at 348 ± 3 K before data acquisition. Each test condition was stabilized before measurements were recorded, and fuel lines were flushed when the liquid fuel was changed.

Instrumentation and Calibration

Cylinder pressure was measured using a water-cooled piezoelectric pressure transducer fitted in the cylinder head. The signal was conditioned through a charge amplifier and synchronized with an incremental crank-angle encoder of 0.1°CA resolution.

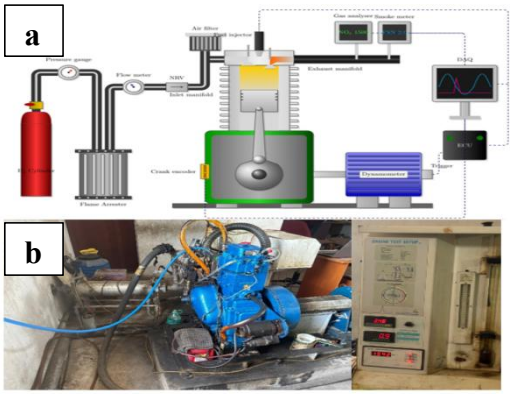

Fig.-4: (a) Schematic Layout of the Experimental Facility (b) Photographic View of the Engine Test Cell

Table-3: Engine Specifications and Imposed Operating Conditions during Steady-State Tests

Parameter	Value	Unit
Engine configuration	4-S Single Cylinder natural aspirated water-cooled	—
Bore	0.0875	m
Stroke	0.110	m
Displacement	6.61×10^{-4}	m^3
Compression ratio	17.5:1	—
Speed set point	25	s^{-1}
Injector opening pressure	20×10^6	Pa
Start of injection	23	°CA BTDC
Load points	25, 50, 75, 100	% rated
Approximate BMEP	0.15, 0.30, 0.45, 0.60	MPa
Hydrogen energy share	0, 5, 10	%
GO dose	0, 50, 100	mg/kg

Exhaust NOx, CO, CO_2, and unburned hydrocarbons were measured using calibrated gas analyzers based on chemiluminescence, non-dispersive infrared, and flame ionization detection methods. Smoke was measured with an opacity-based smoke meter and reported as a filter smoke number. The exhaust sampling probe was fixed downstream of the exhaust valve, and heated sampling lines were used where condensation control was required. Torque was calibrated with a lever arm and traceable dead weights, and dynamometer linearity was checked at three torque settings. Liquid fuel flow was calibrated gravimetrically over a timed interval. The hydrogen mass flow controller was checked against an independent volumetric flow standard. Gas analyzers were zeroed with high-purity nitrogen before each test sequence, and the sensitivity of the pressure transducer was verified using a deadweight pressure calibrator.

Performance and Combustion Calculations

(i) Energy contribution of fuels

Energy = Mass fraction × calorific value

Waste plastic oil = 0.812 X 40 = 7.28MJ

Diesel = 0.727 X 43 =31.26 MJ

Hydrogen = 0.091 X 120 =10.92 MJ

(ii) Brake Power (BP)

Brake power was computed from the torque and speed of the engine using Equation (3), and brake mean effective pressure was obtained using Equation (4).

$$BP = 2\pi NT \quad (3)$$

$$BMEP = 4\pi T / V_d \quad (4)$$

In Equations (3) and (4), brake power is in KW, N is rotational speed in sec, T is braking torque in Nm, and V_d is displacement volume in m^3.

(iii) Brake Thermal Efficiency

Brake thermal efficiency was calculated from the combined chemical energy input using Equation (5).

$$\eta = BP / (\dot{m}1 \times LHVl + \dot{m}H_2 \times LHV^*H_2) \times 100 \quad (5)$$

(iv) Heat Release Rate

The apparent net heat release rate was calculated from averaged cylinder pressure data using a single zone first law model. Instantaneous cylinder volume was obtained from slider-crank geometry, and the heat release rate was calculated using Equation (6).

$$dQnet/d\theta = [\gamma(\gamma-1)]\, p\, (dv/d\theta) + [1/(\gamma-1)]\, V(dp/d\theta) \quad (6)$$

In Equation (6), Q_{net} is the apparent released heat in J, θ is the crank angle in rad, γ was set to 1.35, 'P' is cylinder pressure in Pa, and V_d is cylinder volume in m^3. For each operating condition, 200 successive pressure cycles were recorded and averaged before combustion analysis. Ignition delay was determined through rank angle duration between start of injection and sustained positive heat release. CA50 was determined from cumulative heat release at 50% of the total apparent released heat.

Uncertainty Analysis

The propagation of uncertainty was measured by using the root-mean-square method for independent measurements, as expressed in Equation (7).

$$U\_R = [\sum((\partial R/\partial x_i) \times Ux_i)^2]^{\wedge}(1/2) \quad (7)$$

In Equation (7), U_R is the cumulative uncertainty of the calculated response R, X_i is independent measured variable, and Ux_i is the standard uncertainty of x_i. Repeatability was checked by repeated measurements at similar operating conditions, and all reported calculations were based on stabilized data windows. No human, animal or biological subjects were involved; ethical approval was not required.

RESULTS AND DISCUSSION

Fuel Characterization

Fourier Transform Infrared Spectroscopic (FTIR) Analysis

In diesel, large absorption peaks are observed between 2953 cm^{-1} and 2921 cm^{-1}, related to asymmetric stretching vibrations of (–CH_3, CH_2–) functional groups and the peak at 2853 cm^{-1} is associated with C-H symmetric stretching of alkanes. Additionally, the band observed around 1458 cm^{-1} corresponds to CH_2 bending vibrations, confirming the existence of aliphatic hydrocarbons. Similar peaks were observed for the WPO20D80 blend. This indicates that the dominant hydrocarbon backbone remains intact after blending 20% waste plastic oil with diesel. The appearance of bands in the range of 900-700 cm^{-1} is associated with C=C bending vibrations, indicating the presence of alkenes and aromatic rings, originating from waste plastic oil.

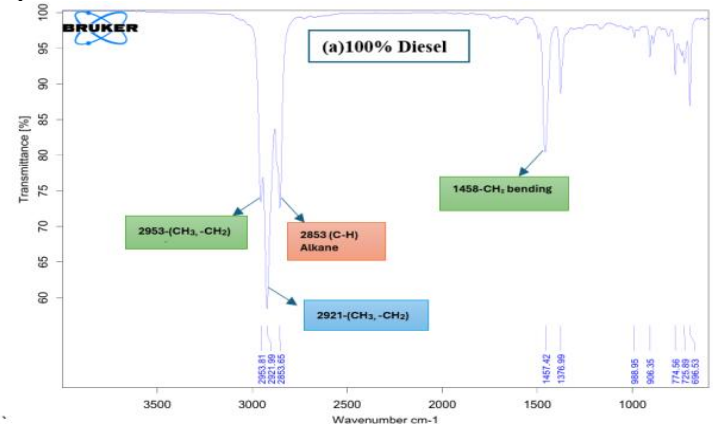

Fig.-5: FTIR Spectrum of Diesel

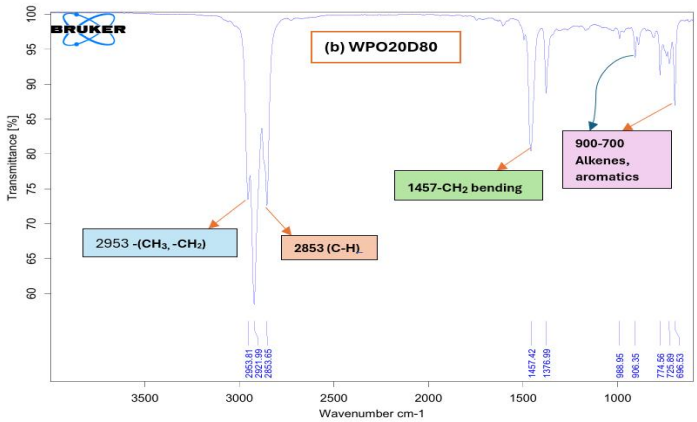

Fig.-6: FTIR Spectrum of 20% WPO + 80% Diesel

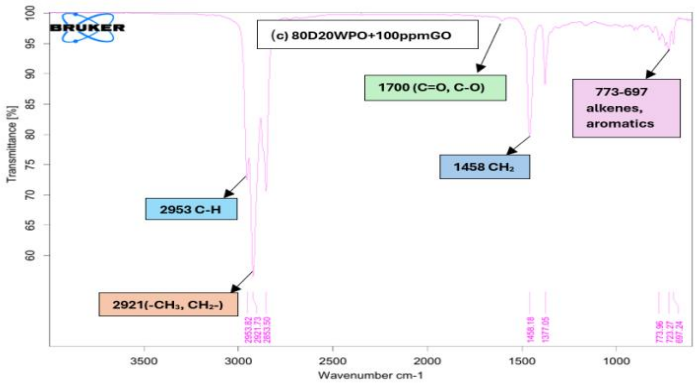

Fig.-7: FTIR Spectrum of 20% WPO + 80% Diesel with 100 ppm GO Nanoparticles

The existence of these compounds slightly increases the chemical complexity compared to diesel fuel, although no prominent oxygenated peaks were found, implying that the blend remains largely hydrocarbon in origin. After incorporation of graphene oxide (GO) nanoparticles, the spectrum of WPO20D80 + GO exhibits prominent changes; particularly, the peak around 1700 cm^{-1} is attributed to C=O (carbonyl) and C-O stretching vibrations, indicating oxygenated functional groups present in the fuel matrix. In addition, the peaks in the region of 773-697 cm^{-1} demonstrate improved aromatic content or interaction effects of GO nanoparticles. Conclusively, the FTIR analysis confirms successful blending of WPO with diesel and indicates that the inclusion of GO nanoparticles adds oxygen-containing functional groups without appreciably affecting the base hydrocarbon structure.

UV-Vis Spectrophotometer Analysis

The UV-Visible absorbance spectra were taken in the range of 200-400nm using the base diesel as the blank and WPO20D80 blended with 100 ppm graphene oxide (GO) as the sample. Diesel showed a very low and nearly flat profile, indicating the absence of strong chromophore groups and confirming the dominance of saturated hydrocarbons with limited π-electron transitions.

On the contrary, the WPO20D80+GO100 ppm sample shows a significant increase in absorbance, particularly in the ultraviolet region between 220 and 320 nm region with a characteristic peak around 219 nm, which is due to π-π* electronic transitions indicating the presence of aromatic C=C bonds or unsaturated compounds within the plastic oil fraction. The n-π* transitions are associated with oxygenated functional groups such as carbonyls. On the other hand, a progressive rise in absorbance beyond 300 nm suggests improved dispersion and interaction of GO within the fuel matrix.

Performance Attributes

Brake Thermal Efficiency (BTE)

Figure-9 illustrates the change in brake thermal efficiency across the load range for five fuel conditions. The distinctions among the fuels become more evident at full load. Under these conditions, blend

WPO20+H_2+GO achieves a BTE of 34.4%, which is approximately 3.6% more than WPO20 and 2.3% higher than diesel fuel.

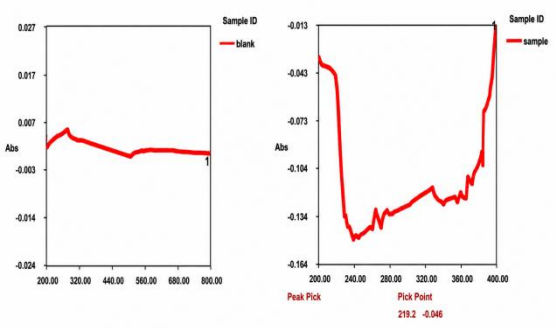

Fig.-8: UV-Visible Spectrum

In comparison, blend WPO20 records a 30.8% BTE, indicating a 1.3% lower value than the neat diesel. This reduction is attributed to lower calorific value, delayed heat release and incomplete oxidation of heavier aromatic constituents.

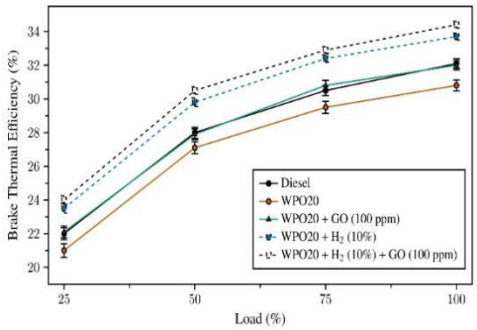

Fig.-9: Brake Thermal Efficiency Versus 25-100% Load for all Fuel Conditions

The incorporation of graphene oxide (GO) nanoparticles significantly mitigates this efficiency deficit. In the case of the WPO20+GO blend achieves 32.0% at full load, falling 0.1% lower than the diesel fuel, indicating that 100 ppm of oxygenated graphene oxide (GO) nanoparticles can effectively compensate for low cetane deficiency loss. Hydrogen enrichment exerts a stronger influence at higher loads; blend WPO20+H_2 reaches 33.7% BTE at full load, and the addition of GO nanoparticles contributes a further improvement of 0.7%. At lower loads, the relative improvements are even more evident; WPO20+H_2+GO recorded roughly 24.0% BTE at 25% load, compared to 21.0% for WPO20. This enhancement is probably attributed to hydrogen-assisted reaction kinetics, which helps to suppress lean quenching and incomplete combustion losses.

Brake Specific Fuel Consumption (BSFC)

Figure-10 illustrates the effect of BSFC with engine load. At maximum load, blend WPO20+H_2+GO reaches 238 g kW/h, which is about 43 g kW/h lower than WPO20 and 30 g kW/h below straight diesel, indicating significant improvement.

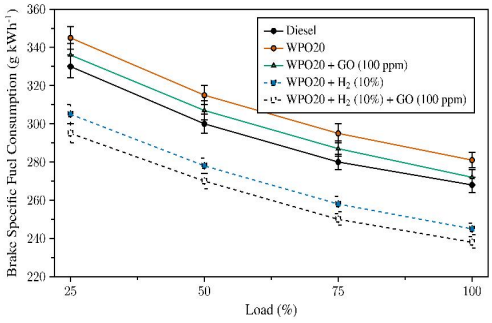

Fig.-10: Change in Brake Specific Fuel Consumption with Engine Load

In contrast, blend WPO20 exhibits the highest fuel consumption across all loads, reaching roughly 345 g kW/h at 25.0% load and declining to 281 g kW/h at full load. In comparison, diesel fell from about 330 to 268 g kW/h over the same range, so the WPO20 full load was approximately 13 g kW/h or 4.9% higher than diesel. This is owing to delayed ignition, lower calorific value and sluggish oxidation of the heavier plastic oil fractions. Adding 100 ppm GO trimmed full-load BSFC to about 272 g kW/h; hydrogen did the heavy lifting, WPO20+H_2 dropped to roughly 245 g kW/h, and the combined condition pushed it down another 7 g kW/h.

Combustion Attributes

In-Cylinder Pressure

Figure-11 (a–b) illustrate the comparative full load combustion intensity across five fuel cases. Diesel exhibits a peak pressure of 65.8 bar and a 3.0 bar °CA^{-1} rise rate, reflecting smooth and well-phased heat release under the baseline conditions. In contrast, blend WPO20 increased to 71.1 bar and 4.0 bar °CA^{-1}, an 8.1% rise in peak pressure was noticed primarily on the account of longer ignition delay of the plastic oil fraction, which promotes greater premixed charge accumulation before combustion started and releases energy abruptly. The addition of GO softened this effect, with WPO20+GO recording 70.4 bar and 3.5 bar °CA^{-1}, suggesting that nanoparticle-assisted ignition reduces the severity of premixed combustion rise without eliminating it.

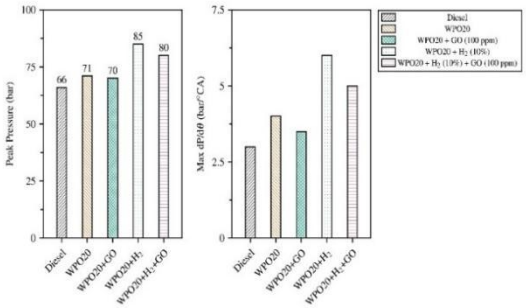

Fig.-11: (a) Maximum In-Cylinder Pressure (b) Peak Pressure Rise Rate at Full Load for all Fuel Formulations

The effect of graphene oxide (GO) was relatively small but consistent. Hydrogen enrichment significantly altered the combustion characteristics. The blend WPO20+H_2 achieved a peak cylinder pressure of 85.1 bar, about 29.3% higher than diesel, along with a pressure rise rate of 6.0 bar °CA^{-1}. This indicates highly intense combustion that may pose challenges related to engine durability, mechanical stress and noise. The coupled effect of hydrogen and graphene oxide (GO) nanoparticles in blend WPO20+H_2+GO brought the peak back to 80.0 bar, and the rise rate decreased to 5.0 bar °CA^{-1} reductions of 5.1 bar and 1.0 bar °CA^{-1} compared to the hydrogen case. This indicates GO functions as a combustion intensity buffer; it effectively dampens the harshest hydrogen peak while preserving the accelerated heat release phasing. This contrasting behavior was observed in Fig.-11. a and 11 b indicate a promising pathway for future engine regimes.

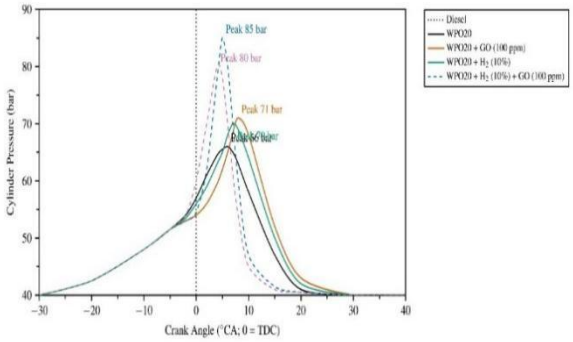

Fig.-12: In-Cylinder Pressure Profile Variation with Crank Angle at Full Load

The moderated pressure profile provides a starting point for retard injection timing or mild EGR without excessive mechanical stress. The exact balance between GO dose and pressure rise softening deserves a dedicated parametric investigation.

Figure-12 shows variation of In-cylinder pressure with crank angle at full load for neat diesel and blends WPO20, WPO20+GO, WPO20+H_2 and WPO20+H_2+GO. All five fuel conditions follow a similar trend during the compression stroke prior to TDC but diverge significantly after combustion starts. This indicates that variations are primarily governed by fuel reactivity and heat release phasing rather than compression effects. Diesel attains a peak pressure of about 66 bar at around 6°CA ATDC. In contrast, blend WPO20 increase the peak pressure to 71 bar and shifts to nearly 8°CA ATDC. This rise of about 5 bar, along with a delay of 2°CA, reflects a longer ignition delay that allows more premixed charge accumulation and combustion during the early expansion phase instead of near TDC. With hydrogen addition, the blend WPO20+H_2 reaches a significantly higher peak pressure of 85 bar at 5°CA ATDC, representing nearly 29% higher than the diesel value. This is due to the rapid combustion of the premixed hydrogen-air fuel mixture, burned fast after pilot ignition, resulting in a shortened the heat release duration. For the blend WPO20+H_2+GO, the peak pressure is moderate round 80 bar and occurs slightly earlier, advancing by about 2°CA compared with the hydrogen case. This indicates that GO promotes the autoignition of heavier WPO molecules and smooths the transition from pilot ignition to premixed combustion. Overall, the results highlighted that hydrogen significantly intensifies the pressure rise and graphene oxide (GO) nanoparticles help to regulate this effect without losing the beneficial combustion phasing advantage.

Heat Release Rate (HRR)

Figure-13 presents a significant difference in heat release rate (HRR) among the fuels during the premixed combustion phase. Diesel exhibits a peak HRR of about 99 kJ °CA^{-1} near 2°CA ATDC, followed by noticeable diffusion combustion stretch beyond 20°CA ATDC. In contrast, blend WPO20 rise the peak HRR to 121kJ°CA^{-1}, representing roughly a 22% rise and shifts it to nearly 4°CA ATDC. This behaviour reflects a longer ignition delay, allows accumulation of a larger premixed charge and releases energy later than the optimum crank angle.

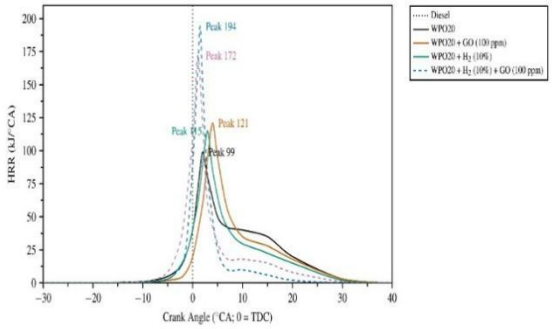

Fig.-13: Variation of Heat Release Rate with Load for all Fuel Configurations

The addition of graphene oxide (GO) nanoparticles moderates this effect blend WPO20+GO demonstrates a down-fall peak around 110 kJ°CA^{-1}, reflecting more controlled combustion. The blend WPO20+H_2 produces a sharp peak of around 194 kJ °CA^{-1} at 1.5°CA ATDC, which is roughly 96% higher than diesel and 60% above the WPO20, while the diffusion combustion phase almost disappears. This indicates that hydrogen accelerates flame propagation and promotes rapid consumption of carbon-rich spray, leaving little fuel for late diffusion combustion. For the blend WPO20+H_2+GO combination, the peak HRR is reduced to approximately 172 kJ °CA^{-1}, representing an 11% reduction compared to the hydrogen case alone, while maintaining early combustion phasing near 1°CA ATDC. This indicates GO shortens the ignition delay and redistributes the heat release across a slightly wider crank-angle range, rather than concentrating it into a sharp peak. This characteristic is important for NO formation, as peak combustion temperatures are strongly influenced by heat release intensity. A 11% reduction in peak HRR

can curb thermal NO formation. Furthermore, mixing of H_2+GO with slight injection timing retardation or mild EGR could preserve the compact combustion profile, while reducing peak temperature exposure.

Ignition Delay

Figure-14 (a–b) demonstrates the decoupled roles of GO and hydrogen in controlling combustion timing. In Fig.-14(a), ignition delay decreases with load for all cases from 14.5°CA to 12.0°CA for WPO20, as expected due to rising in-cylinder temperature. However, WPO20 remains well above the diesel reference (near 8°CA), reflecting the poorer autoignition quality of the plastic oil blend. The addition of 100 ppm GO consistently reduces ignition delay by about 2°CA across all the loads, bringing the full load value to 10.0°CA, a 16.7% reduction.

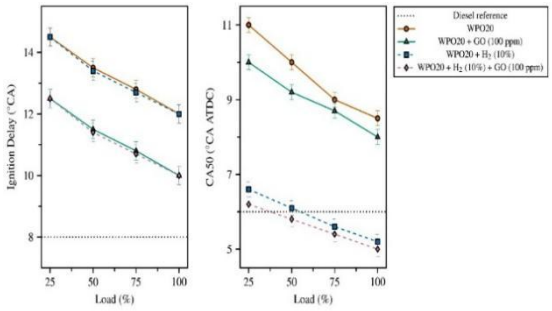

Fig.-14: (a) Ignition Delay (b) CA50 Verses Load

This was not anticipated to be so uniform a load dependent response was expected. GO promotes surface-catalysed ignition of heavier WPO fragments regardless of thermal environment. In contrast, hydrogen showed almost no change in ignition delay, with the WPO20+H_2 curve tracking WPO20 within 0.1-0.2°CA, because the start of combustion is governed by liquid pilot autoignition, not gaseous fuel reactivity. In Fig.-14 (b), the story flips: CA50 for WPO20 decreases from 11.0°CA ATDC at 25% load to 8.5°CA ATDC at maximum load, yet remains later than the optimal 5-7°CA efficiency band. GO provides only a slight advancement, bringing CA50 to around 8.0°CA at full load. Hydrogen provides the primary shift: WPO20+H_2 achieves 5.2°CA ATDC at full load, and the combined WPO20+H_2+GO condition pushed it to 5.0°CA ATDC, placing all load conditions within the desired range. In summary, GO shortens ignition delay and hydrogen advances CA50. These are different mechanisms acting on different phases of combustion, a distinction that has implications for injection strategy.

Emission Attributes

NOx Emissions

Figure-15 shows that as engine load increased, NOx emissions rose in all cases predictably, but the magnitude varied across fuels. All cases increased from roughly 400-600 ppm at 25% load to 1100-1500 ppm at maximum load, driven by higher in-cylinder temperatures and longer residence times within the thermal NO formation regime. Diesel followed a baseline trend, rising from 400 to 1100 ppm.

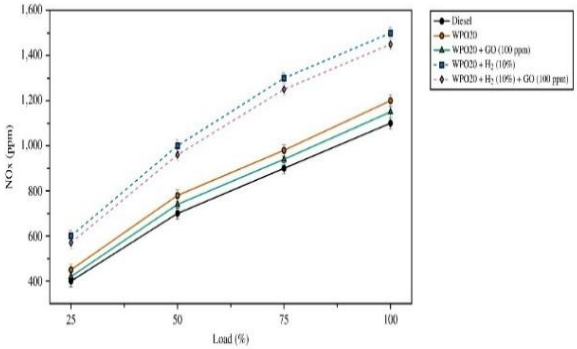

Fig.-15: NOx Emissions Across Load for all Fuel Formulations

In contrast, WPO20 climbed above diesel at every point and reached 1200 ppm at full load, a 100 ppm or 9.1% increase that ties back to stronger premixed combustion from longer ignition delay. In addition to GO, NOx was mitigated slightly by 50 ppm, whereas the WPO20 curve at full load is about 1150 ppm, a 4.2% cut. Hydrogen recorded a significant rise in NOx emissions; WPO20+H_2 reached roughly 1500 ppm at full load, about 300 ppm higher than WPO20 and 400 ppm above the diesel, corresponding to a 36.4% higher than the diesel. The combined WPO20+H_2+GO condition pulled back to about 1450 ppm; a 50 ppm, or 3.3%, reduction was noticed. It is a mild reduction; further mild EGR can bridge the remaining gap without affecting the smoke. A similar trend of NOx escalation with hydrogen-enriched WPO has been reported by Anand and Debbarma in a CRDI engine.[13]

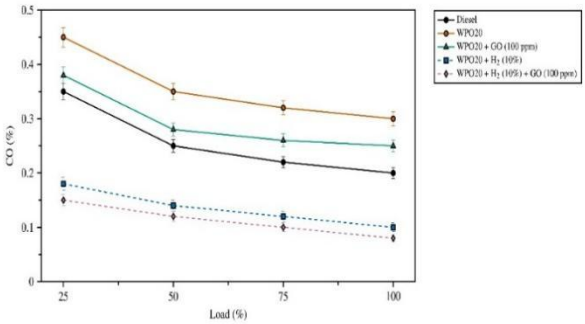

Fig.-16: CO Emissions Across the Load for all Fuel Formulations

Figure-16, presents the variation of carbon monoxide emissions for all tested fuel conditions, showing both expected and striking results. WPO20 fuel consistently delivers the highest CO emissions throughout the load range, with values around 0.45% at 25% load and dropping to 0.30% at maximum load. In contrast, diesel records lower emissions, about 0.35% at low load and 0.20% at full load. The resulting full-load CO gap of 0.10% is a relative increase of 50% for WPO20, mainly due to slower oxidation rates of the heavier molecules of plastic oil, notably in locally fuel-rich spray regions. Incorporating GO nanoparticles into the WPO20 blend leads to a steady improvement in the reduction of CO emissions to around 0.25% at full load. This corresponds to a 16.7% decrease, indicating that GO contributes modestly but reliable effect on facilitating more complete oxidation of fuel molecules. The effect of hydrogen enrichment is considerably more substantial. At full load, hydrogen addition (WPO20+H_2) CO emission levels dropped sharply to about 0.10%. While GO was combined with hydrogen (WPO20+H_2+GO), CO dropped further to approximately 0.08%, a reduction of 73% relative to WPO20 and 60% compared to diesel. At low load conditions, the reduction of CO with the WPO20 blend becomes more pronounced records around 0.45% CO, whereas the WPO20+H_2+GO combination reached about 0.15%. This substantial reduction in CO emissions can be attributed to accelerated flame propagation and a rich concentration of reactive radicals, particularly hydroxyl (OH) groups, which facilitate more oxidation of fuel molecules and effectively convert CO to CO_2 before expansion. The consistently low CO levels attained in the H_2+GO cases also provide a valuable margin for future NOx reduction strategies.

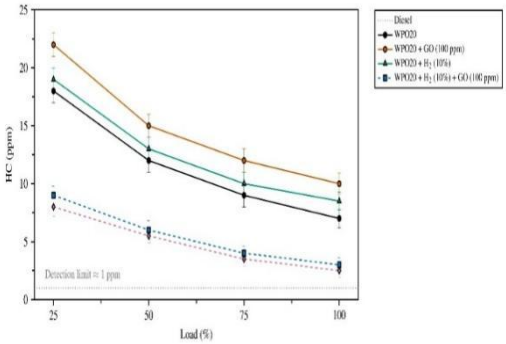

Fig.-17: Unburned HC Emissions Versus Load for all Fuel Conditions

Figure-17 shows the behavior of unburned hydrocarbon emissions with engine load. Diesel declined from about 18 ppm at 25% load to 7 ppm at maximum load. WPO20 remains above diesel across all loads and reached 10 ppm at full load, a 3ppm increase or approximately a 43% rise. The heavier plastic oil components produced slower oxidation and left persistent heavy hydrocarbon fragments in wall cooled or locally rich spray zones. In addition, GO improves oxidation and lowers HC emissions from 10 ppm to 8.5 ppm, a 15% decrease that aligns with oxygenated functional groups promoting late-burn oxidation. The hydrogen effect was dominant; the WPO20+H2 blend shows 3 ppm at full load, depicting a 70% reduction compared to WPO20 and 57% lower than diesel. The WPO20+H_2+GO blend achieved a low level of emissions of about 2.5 ppm, although this reduction is well above the threshold limit of 1 ppm, indicating that the improvement is experimentally significant. At a lower 25% load, WPO20+H_2+GO recorded about 8 ppm, while WPO20 was near 22 ppm; a gap of 14 ppm, and the difference is even more pronounced. The behaviour is straightforward: hydrogen-driven flame propagation reaches crevice and wall-adjacent regions faster, converting hydrocarbons before expansion cooling arrests the reaction.

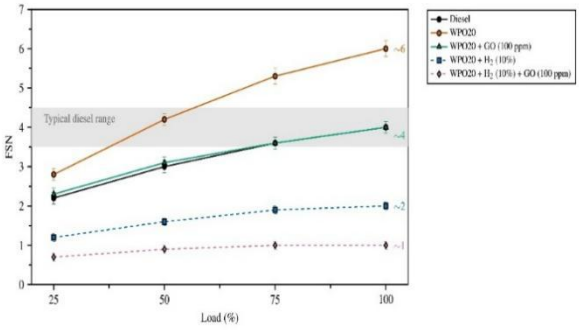

Fig.-18: Smoke Opacity (FSN) with Load for all Fuel Conditions

Figure-18 presents one of the most striking outcomes, showing the hydrogen-GO combination effectively suppresses the visible smoke. At full load, WPO20 produced nearly 6.0 FSN, about 2.0 FSN higher than diesel or 50% higher, primarily due to the higher number of aromatic components in plastic oil, longer ignition delay and sluggish soot oxidation. The addition of GO cut this to about 4.0 FSN; a 33% reduction was attained, which is close to the diesel. Hydrogen had the most pronounced effect: the WPO20+H_2 case smoke emission drops to approximately 2.0 FSN, while the combined WPO20+H_2+GO configuration further reduced it to 1.0 FSN at full load. An 83% reduction compared to WPO20, 75% lower than the diesel. Importantly, the separation between these curves exceeds the repeatability band of about ±0.2 FSN at every load point. At 25% load, WPO20+H_2+GO recorded approximately 0.7 FSN while WPO20 was near 2.8 FSN. The mechanism follows different pathways: one is that hydrogen dilutes the carbon-rich diffusion flame and provides OH radicals that aid in oxidizing soot particles, and graphene oxide nanoparticles (GO) enhance surface-catalyzed oxidation reactions within the diffusion combustion zone. This near smokeless operation is the most practically valuable finding, as it provides a large margin to absorb any EGR-related smoke increase during future NOx control strategies.

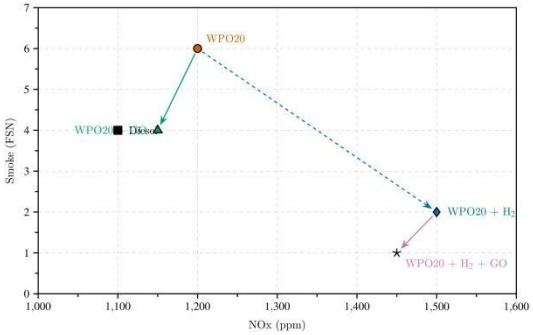

Fig.-19: Full Load NOx-Smoke Positioning for all Fuel Configurations

Figure-19 comprises the key NOx-Smoke trade-off in a single plot. Diesel sits near 1100 ppm NOx and 4 FSN, the reference anchor. WPO20 shifts to a clearly inferior region, reaching about 1200 ppm NOx and 6 FSN; both the emissions worsen due to longer ignition delay, intensified premixed combustion and heavier soot formation. GO pulls WPO20 back toward the diesel zone emissions to around 1150 ppm NOx and 4 FSN, a clear improvement on both axes at the same time. Hydrogen produces a dramatic smoke drop down to 2 FSN, but a steep rise in NOx reaches to 1500 ppm. The combined WPO20+H_2+GO lands at 1450 ppm NOx and 1 FSN, reflecting a 50 ppm NOx and 1 FSN smoke cut from the addition of hydrogen. The position is far from diesel on the NOx axis, but the near-zero smoke margin is remarkable.

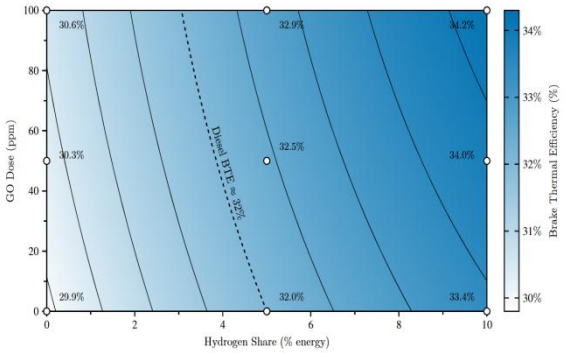

Fig.-20: Response Surface Contour of BTE under 75% Load as a Function of Hydrogen Share & GO Dose

Figure-20 presents the optimization surface for brake thermal efficiency at 75% load and shows how BTE varies with respect to hydrogen energy share and GO. The gradient is much steeper along the hydrogen axis, indicating that hydrogen share is the dominant control variable for efficiency improvement. At the baseline condition of 0% hydrogen and 0 ppm GO, BTE sits at 29.9% of the WPO20 baseline deficit. Increasing GO alone raises BTE to only about 30.6% at 100 ppm, an improvement of approximately 0.7 points. Addition of hydrogen produces a substantial improvement; at 5% hydrogen energy share, BTE rises to about 32.0% without GO and 32.9% at 100 ppm GO. At 10% hydrogen share, BTE further increases and attains 33.4% without GO and 34.2% with 100 ppm GO. The diesel reference of about 32% is crossed near 4-5% with hydrogen and GO addition. This indicates inclusion of GO nanoparticles lowers the hydrogen demand for diesel-equivalent efficiency by approximately 20-30%. The response surface method also reveals diminishing returns beyond 80 ppm GO, particularly at high hydrogen fraction. An optimal operating region lies at 5-8% hydrogen share and 80-100 ppm GO, where BTE ranges from 33-34%.

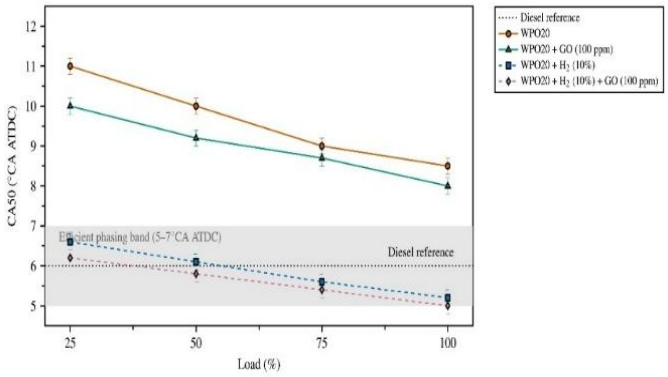

Fig.-21: CA50 Combustion Phasing Relative to 5-7ºCA ATDC High-Efficiency Band Across Load

Figure-21 provides clear practical insight: hydrogen acts as the key factor that shifts WPO20 combustion into the optimal phasing region, while GO contributes a little additional advance. The blend WPO20 remains outside the desired 5-7°CA ATDC range at all loads, ranging from 11.0°CA at 25% load to

8.5°CA at full load. This consistent retarded combustion phasing accounts for the lower BTE observed in Figure 9. In addition, GO nanoparticles result in only modest advancement in CA50, reaching about 10.0°CA at low load and 8.0°CA at full load, which is still under the target range. In contrast, hydrogen significantly alters the combustion phasing of the WPO20 blend, bringing CA50 into the optimal conditions across all loads. The blend WPO20+H_2 falls roughly at 6.6°CA at 25% load, 6.1°CA at 50%, 5.6°CA at 75%, and 5.2°CA at full load. The combined WPO20+H_2+GO configuration advances CA50 slightly earlier by 0.2-0.4°CA at each load point, reaching 5.0°CA ATDC at full load. This shift is small but consistent and significant; it is only the case of full load CA50 aligns with the lower boundary of the optimal range. One concern: at 5.0°CA ATDC, combustion is already early enough that any further advance would push heat release before TDC, raising negative work on the piston. So, the combined H_2+GO condition is close to the optimum phasing limit at full load, and a slight injection retard or mild EGR rate would be needed to keep CA50 centered in the band rather than drifting below it.

CONCLUSION

The present investigation assessed combustion, performance and emission behavior of WPO-Diesel blends upgraded through graphene oxide nanoparticle dispersion and controlled hydrogen induction on a four-stroke single-cylinder direct injection diesel engine. The results showed that the performance deficit associated with WPO20 was substantially recovered when hydrogen and GO were applied together. At full load, brake thermal efficiency had reached 34.4%, compared with 30.8% for WPO20, while brake-specific fuel consumption had declined from 281 to 238 g kWh^{-1}. These gains confirmed that accelerated hydrogen-supported combustion and GO-assisted oxidation acted cooperatively to improve the utilization of the WPO-containing fuel. Hydrogen produced the dominant advancement in combustion phasing and shifted CA50 from 8.5°CA ATDC for WPO20 to approximately 5.2°CA ATDC. However, the resulting rapid premixed combustion raised peak cylinder pressure to 85.1 bar, pressure-rise rate to 6.0 bar $°CA^{-1}$, and peak heat-release rate to 194 kJ $°CA^{-1}$. When GO was introduced together with hydrogen, these values were moderated to 80.0 bar, 5.0 bar $°CA^{-1}$, and approximately 172 kJ $°CA^{-1}$, respectively. GO had also shortened the WPO20 ignition delay from 12.0°CA to 10.0°CA. The combined condition had therefore retained favorable combustion phasing while reducing the severity of the hydrogen-induced combustion peak. The strongest practical benefit had been observed in carbonaceous emissions. Full-load smoke had been reduced from 6 FSN for WPO20 to 1 FSN for WPO20+H_2+GO, corresponding to an 83.0% decrease. Carbon monoxide had fallen from 0.30% to 0.08%, while unburned hydrocarbons had declined from 10 ppm to 2.5 ppm. The principal remaining limitation had been NOx, which had reached approximately 1450 ppm under the combined condition despite being lower than the 1500 ppm recorded with hydrogen alone. The results had therefore indicated that further optimization should have focused on mild EGR, small injection-timing retardation, and coordinated hydrogen share and GO dose calibration so that the near-smokeless operating margin could be used to suppress NOx without sacrificing combustion efficiency. Long-duration investigations had also been recommended to examine injector deposits, filtration requirements, GO suspension stability beyond seven days, component durability, and performance in multicylinder engines. The current study supports broader sustainable development goals, SDG-7 and SDG-13, through waste valorization, reduced dependency on conventional diesel and development of low-carbon combustion strategies.

ACKNOWLEDGMENTS

The authors gratefully acknowledge Aditya University, Surampalem, for providing FTIR and UV–Visible spectroscopy facilities and Sri Venkateswara Consultancy for engine testing facilities.

CONFLICT OF INTERESTS

The authors declare that there is no conflict of interest.

AUTHOR CONTRIBUTIONS

The present work is related to *SDG-7: Affordable Clean Energy*. All the authors contributed significantly to this manuscript, participated in reviewing/editing and approved the final draft for publication. The research profile of the authors can be verified from their ORCID ids, given below:

Rakesh Varma Kadupu https://orcid.org/0000-0002-2109-5307
K. Syed Jafar https://orcid.org/0000-0003-3688-1826
P. V. Elumalai https://orcid.org/0000-0002-7536-8200

Cite this article as: R. V. Kadupu *et al.*, *Rasayan J. Chem.*, 19(3), 1902-1918(2026), https://doi.org/10.31788/RJC.2026.19310019

REFERENCES

1. V. L. Mangesh, S. Padmanabhan, P. Tamizhdurai and A. Ramesh, *Journal of Cleaner Production*, **246**, 119066(2020), https://doi.org/10.1016/j.jclepro.2019.119066
2. M. Mariappan, M. S. Panithasan and G. Venkadesan, *Journal of Cleaner Production*, **312**, 127687(2021), https://doi.org/10.1016/j.jclepro.2021.127687
3. K. Janarthanan and P. Sivanandi, *Journal of Cleaner Production*, **366**, 132924(2022), https://doi.org/10.1016/j.jclepro.2022.132924
4. H. Yaqoob, H. M. Ali, U. Sajjad and K. Hamid, *Results in Engineering*, **24**, 103336(2024), https://doi.org/10.1016/j.rineng.2024.103336
5. M. Sekar, T. R. Praveenkumar, V. Dhinakaran, P. Gunasekar and A. Pugazhendhi, *Journal of Cleaner Production*, **318**, 128551(2021), https://doi.org/10.1016/j.jclepro.2021.128551
6. A. I. El-Seesy, H. Hassan and S. Ookawara, *Energy Conversion and Management*, **166**, 674(2018), https://doi.org/10.1016/j.enconman.2018.04.049
7. J. Li, J. Wei, H. Chen, Y. Xu, Y. Liu and Q. Dai, *Renewable Energy*, **246**, 122941(2025), https://doi.org/10.1016/j.renene.2025.12294
8. R. Estevez, L. Aguado-Deblas, F. J. López-Tenllado, F. M. Bautista, A. A. Romero and D. Luna, *Energies*, **17**, 1322(2024), https://doi.org/10.3390/en17061322
9. L. Razzaq, M. A. Mujtaba, M. E. M. Soudagar, W. Ahmed, H. Fayaz, S. Bashir, I. M. R. Fattah, H. Chyuan, K. Shahapurkar, A. Afzal, S. Wageh, A. Al-Ghamdi, M. Shujaat and A. I. El-Seesy, *Journal of Environmental Management*, **282**, 111917(2021), https://doi.org/10.1016/j.jenvman.2020.111917
10. N. Chacko and T. Jeyaseelan, *Fuel Processing Technology*, **204**, 106406(2020), https://doi.org/10.1016/j.fuproc.2020.106406
11. R. Saaidia, F. Hamdi, M. Krotli, A. Bouabidi, E. Cuce, H. Koten and I. Miraoui, *Renewable Energy*, **241**, 122387(2025), https://doi.org/10.1016/j.renene.2025.122387
12. M.Sekar, *Renewable Energy*, **249**, 123222(2025), https://doi.org/10.1016/j.renene.2025.123222
13. T. Anand and S. Debbarma, *International Journal of Hydrogen Energy*, **57**, 1051(2024), https://doi.org/10.1016/j.ijhydene.2024.01.052
14. S. Özer, H. E. Gülcan, S. Çelebi and U. Demir, *International Journal of Hydrogen Energy*, **143**, 862(2025), https://doi.org/10.1016/j.ijhydene.2024.11.107
15. Y. Wu, Y. Yuan, C. Xia and A. Pugazhendhi, *Fuel*, **355**, 129458(2024), https://doi.org/10.1016/j.fuel.2023.129458
16. A. K. Das, A. K. Acharya, B. Parida, A. K. Panda, Z. Yao and S. Kumar, *Thermal Science and Engineering Progress*, **67**, 104136(2025), https://doi.org/10.1016/j.tsep.2025.104136
17. A. Kumar, H. S. Pali and M. Kumar, *Fuel*, **355**, 129448(2024), https://doi.org/10.1016/j.fuel.2023.129448
18. S. Ma, Q. Guo, J. Wei, Z. Yin, Y. Zhuang, Y. Zhang, Q. Dai and Y. Qian, *Energy*, **300**, 131616(2024), https://doi.org/10.1016/j.energy.2024.131616
19. S. M. Hammad, H. Yaqoob, M. U. Farooq, H. M. Ali, U. Sajjad, M. A. Jamil and K. Hamid, *Energy Conversion and Management: X*, **23**, 100710(2024), https://doi.org/10.1016/j.ecmx.2024.100710
20. T. D. Megiso, V. R. Ancha and R. B. Nallamothu, *Energy Conversion and Management: X*, **28**, 101259(2025), https://doi.org/10.1016/j.ecmx.2025.101259
21. E. R. K. Reddy and M. K. Pal, *International Journal of Hydrogen Energy*, **49**, 1282(2024), https://doi.org/10.1016/j.ijhydene.2023.09.025
22. S. Sarıdemir, F. Polat and Ü. Ağbulut, *Process Safety and Environmental Protection*, **184**, 637(2024), https://doi.org/10.1016/j.psep.2024.02.018 [RJC-10019/2026]